



# Research Repository UCD

<b>Title</b>	In vitro Characterization of an Electroactive Carbon-Nanotube-Based Nanofiber Scaffold for Tissue Engineering
<b>Authors(s)</b>	Mackle, Joseph N., Blond, David J.-P., Mooney, Emma, et al.
<b>Publication date</b>	2011-07-04
<b>Publication information</b>	Mackle, Joseph N., David J.-P. Blond, Emma Mooney, and et al. "In Vitro Characterization of an Electroactive Carbon-Nanotube-Based Nanofiber Scaffold for Tissue Engineering." Wiley Blackwell (John Wiley & Sons), July 4, 2011. <a href="https://doi.org/10.1002/mabi.201100029">https://doi.org/10.1002/mabi.201100029</a> .
<b>Publisher</b>	Wiley Blackwell (John Wiley & Sons)
<b>Item record/more information</b>	<a href="http://hdl.handle.net/10197/5011">http://hdl.handle.net/10197/5011</a>
<b>Publisher's statement</b>	This is the author's version of the following article: Joseph N. Mackle, David J.-P. Blond, Emma Mooney, Caitlin McDonnell, Werner J. Blau, Georgina Shaw, Frank P. Barry, J. Mary Murphy, & Valerie Barron (2011) "In vitro Characterization of an Electroactive Carbon-Nanotube-Based Nanofiber Scaffold for Tissue Engineering" Macromolecular Bioscience, 11 : 1272-1282 which has been published in final form at <a href="http://dx.doi.org/10.1002/mabi.201100029">http://dx.doi.org/10.1002/mabi.201100029</a> .
<b>Publisher's version (DOI)</b>	<a href="https://doi.org/10.1002/mabi.201100029">10.1002/mabi.201100029</a>

Downloaded 2025-12-04 22:45:07

The UCD community has made this article openly available. Please share how this access benefits you. Your story matters! (@ucd\_oa)



© Some rights reserved. For more information

DOI: 10.1002/((please add journal code and manuscript number))

**Article type:** Full Length Article

***In vitro* Characterization of an Electroactive Carbon Nanotube Based Nanofiber Scaffold For Cardiac Muscle Repair**

Joseph N. Mackle<sup>1</sup>, David J-P Blond<sup>2</sup>, Caitlin McDonnell<sup>1</sup>, Werner J. Blau<sup>2</sup>, Emma Mooney<sup>1</sup>, Frank Barry<sup>1</sup> Mary Murphy<sup>1</sup> and Valerie Barron\*<sup>1</sup>

---

Mr. J.N. Mackle, Ms. C. McDonnell, Dr. E. Mooney, Prof. F. Barry, Dr. M. Murphy, Dr. V.Barron

<sup>1</sup>Regenerative Medicine Institute (REMEDI), National Centre for Biomedical Engineering Science (NCBES), Orbsen Building, National University of Ireland, Galway, University Road, Galway, Ireland.

Email: [Valerie.Barron@nuigalway](mailto:Valerie.Barron@nuigalway)

Dr. D. J-P Blond, Prof. W.J. Blau

<sup>2</sup>Molecular Electronics and Nanotechnology Group, School of Physics, Trinity College Dublin, Dublin 2, Ireland.

---

**Keywords:** carbon nanotubes; degradation profile; electroactive scaffolds; mesenchymal stem cell response; polylactic acid

## Abstract

After myocardial infarction, the electroactive cardiac muscle tissue has little intrinsic repair/regeneration capacity. To date, a range of tissue engineering scaffolds have been investigated for myocardial repair, yet many have neglected to address electrical property requirements. To overcome this limitation, a biomimetic carbon nanotube (CNT) based polylactic acid (PLA) nanofibre scaffold is described herein. After 28 days in simulated physiological solutions at 37°C, a change in the mass, chemical properties and polymer morphology is seen. However, the mechanical properties and physical integrity appear unaltered. Furthermore, no adverse cytotoxic effects on the human mesenchymal stem cells (hMSC) are observed. Taken together, these data auger well for electroactive cardiac tissue applications.

## Introduction

The repair of cardiac muscle after myocardial infarction or ischemic heart disease is limited due to the poor regeneration/repair potential of cardiomyocytes in the damaged tissue. Current methodologies which address this problem, include the injection of dissociated myogenic cells into the myocardium. To date, a number of cells have been investigated including embryonic stem cells, bone marrow progenitor cells, and neonatal rat cardiomyocytes.<sup>[1-9]</sup> However, as yet, no optimal cellular therapy has been identified. With respect to tissue engineering approaches, a range of scaffold materials including collagen, matrigel, fibrin and poly(1,8-octanediol-co-citric acid) (POC) have been investigated for myocardium repair,<sup>[10-17]</sup> again with limited success. Therefore, a different approach was adopted in this study. Since cardiac muscle is an electroactive tissue, this research sought to create and characterize an electroactive scaffold. Although, a range of electrically conducting polymers such as polyaniline and polypyrrole have been examined for various tissue engineering applications<sup>[17-21]</sup>, more recently, interest has been growing in carbon nanotubes

(CNT) for biomedical applications.<sup>[22]</sup> Carbon nanotubes are long thin tubes of graphene that are capable of conducting electricity. Their unique electrical and mechanical properties can be exploited to create biomimetic tailored scaffolds. Furthermore, CNT based polymer nanofibers can be produced by electrospinning.<sup>[23]</sup> In parallel, PLA, an FDA approved polymer, can be electrospun to produce random nanofibre scaffolds. Therefore, this study aims to test the hypothesis that electrospun CNT based PLA scaffolds can be created for cardiac muscle applications.

Initially, a range of CNT concentrations were screened to determine the optimum electrical properties. Thereafter, the electrospinning parameters were optimized to produce nanofibers of uniform diameter with an even distribution of CNT. Subsequently, the degradation profile of the CNT/PLA nanofibre scaffolds was examined over a 28-day period. In parallel, the cell viability of the hMSC in the presence of the electrospun scaffolds was examined.

## **2. Experimental Section**

### **2.1 CNT/PLA Nanofibre Scaffold Preparation**

A 30-wt % solution of poly-l-lactide acid (PLA) (Sigma, UK) in a 70:30 mixture of dichloromethane and dimethylformamide was created. Thereafter, the SWNT (Nanocyl, Belgium) were added to the PLA solution to produce various volume fractions from 0 to 2-wt%, as described previously.<sup>[23]</sup> For clarity, the SWNT will be referred to as CNT throughout the article. Subsequently, the electrical properties were examined using a conductivity meter (High Resistance/Low Conductance Meter Alpha Lab, USA), where it was revealed that there was inverse relationship between CNT concentration and resistance; the 2-wt% sample had the lowest resistance with a value of  $7 \times 10^{-6} \Omega$ . Above 2-wt%, the values began to plateau, and as a result, a 2-wt% SWNT/PLA solution was used to create the electrospun randomly oriented nanofibre scaffolds using a voltage of 15kV and a feed rate of 0.05 ml/min, with the

collector screen 15cm from the syringe needle. As a method of control electrospun randomly oriented PLA nanofibre scaffolds were also produced without CNT.

## **2.2. Degradation Profile of the CNT/PLA Nanofibre Scaffold**

To examine the degradation profile of the scaffolds, specimens were stored in a physiological solution, that is, phosphate buffered solution (PBS: 0.138 M NaCl, 0.0027M KCl, pH 7.4) (Sigma, UK) at 37°C and their materials properties were examined over a 28-day period. Subsequent changes in the mass of the CNT/PLA nanofibre scaffolds, pH of the solutions, chemical properties, polymer morphology and mechanical properties were examined as described below. As a method of control PLA nanofibre scaffolds without CNT were also stored in the same solutions.

### **2.2.1. Gravimetric Analysis**

The materials properties of the scaffolds were examined over a 28-day period on days 0,7,14 and 28 respectively. The scaffolds were removed from the solutions, rinsed with deionized water and dried with a tissue. After allowing the pieces to dry at room temperature for 5 min. the mass was determined on a microbalance (Sartorius CP64, Germany) (n=10). The change in mass ( $\Delta M$ ) was determined using equation 1, where  $M_f$  is the final mass of the sample that was removed from the solution and dried for 5 min. and  $M_i$  is the initial mass of the sample.

$$\Delta M(\%) = \frac{M_f - M_i}{M_i} \times 100\% \quad (1)$$

As a method of control, samples were stored in a dry atmosphere at 37°C (n=10). Once the samples were removed from the solutions the pH was measured using a pH meter (HI-112 Bench pH meter, Hanna Instruments, UK) to evaluate potential changes due to the degradation of the CNT/PLA nanofibre scaffolds. In parallel, the pH of the solutions containing PLA nanofibre scaffold and solutions containing no scaffolds was measured as a

method of control. To determine whether the CNT diffused into the PBS solution, RAMAN (HORIBA Jobin Yvon Labram HR, UK) spectroscopy was employed to detect the presence of CNT in the solutions.

### 2.2.2 Chemical Property Evaluation

Since the PLA matrix material is biodegradable, the chemical structure of the CNT nanofibre scaffolds stored in PBS was evaluated on day 0, 7, 14 and 28 using Fourier transform infra red spectroscopy (FTIR-8300 Shimadzu, UK,). As before, specimens were taken out of the PBS solution, rinsed in deionized water and dried in a dessicator at room temperature for 24h. Spectra were recorded in the wavelength range of  $4000$  to  $400\text{cm}^{-1}$  by  $2\text{cm}^{-1}$  resolution in 32 scans. Spectra were recorded in ten different areas of each specimen ( $n=6$ ) and normalized to the intensity of peak at  $1450\text{cm}^{-1}$  for CH stretching in the  $\text{CH}_3$  group. To ensure that there were effects due to varying sample thickness, the samples were measured before and after the immersion and drying procedure.

### 2.2.3 Polymer Morphology Examination

To determine if the crystalline structure of the CNT nanoscaffolds changed over the 28-day period in PBS at  $37^\circ\text{C}$ , the thermal properties of the materials were examined using differential scanning calorimetry (DSC 60, Shimadzu, UK). Samples were taken out of the PBS solution, rinsed in deionized water and dried in a dessicator at room temperature for 24h. 5 mg of each sample was heated at a rate of  $10^\circ\text{C}/\text{min}$  from room temperature to  $200^\circ\text{C}$ . A typical DSC thermogram for CNT/PLA scaffold is shown in Figure 3A from which it was possible to determine the glass transition temperature ( $T_g$ ), crystallization temperature ( $T_c$ ) and the crystalline melt temperature ( $T_m$ ) for each sample on day 0, 7, 14 and 28 ( $n=5$ ). The percentage crystallinity ( $\chi\%$ ) was also determined for each time point using equation 2 and a value of  $87\text{J/g}$  for the heat of fusion ( $\Delta H_F$ ) for a pure PLA crystal.<sup>[37]</sup> The heat for the

crystalline melt region ( $\Delta H_m$ ) was determined by measuring the area under the curve.

$$\chi(\%) = \frac{\Delta H_m}{\Delta H_F} \times 100\% \quad (2)$$

#### 2.2.4 Mechanical Property Evaluation

Tensile specimens similar to that described previously were produced with dimension of 25mm X 25mm X 0.15 mm and stored in PBS.<sup>[14]</sup> On days 0, 7, 14 and 28, the scaffolds were taken out of the PBS solution, allowed to dry on a sheet of tissue paper for 5 min. and cool down to room temperature. Thereafter, specimens were tensile tested until failure using a Zwick Z100 tensile tester (Zwick, Germany) using a 100N load cell with a crosshead speed of 0.5mm/min. Stress-strain curves were generated, from which it was possible to determine the tensile strength at break ( $\sigma_{TS}$ ), elongation at break ( $\epsilon$ ), where  $\epsilon$  is calculated using equation 3 and Youngs modulus (E) by measuring the slope of the elastic region of the curve (n=10).

$$\epsilon(\%) = \frac{\Delta l}{l_i} \times 100\% \quad (3)$$

$\Delta L = l_f - l_i$  where,  $l_f$  is the final length and  $l_i$  is the initial length of the test specimen.

Typical stress-strain curves are shown in Figure 4A for the PLA control and the CNT/PLA scaffolds.

#### 2.2.5 Scanning Electron Microscopy

To determine whether there was any visible physical degradation of the nanofibre scaffolds stored in PBS at 37°C over the 28-day period, samples were examined using SEM (Hitachi S-4700, UK). As before, specimens were taken out of the PBS solution, rinsed in deionized water, dried in a dessicator at room temperature for 24h. and sputter coated with gold prior to examination.

## **2.3 hMSC Viability in the presence of the CNT/PLA Nanofibre Scaffold**

### **2.3.1 hMSC Isolation and Confirmation of Phenotype**

hMSC were isolated from the adult bone marrow as described previously.<sup>[38]</sup> In brief, a 30ml aspirate of bone marrow was obtained from the iliac crest of healthy volunteers. The aspirate was heparin treated and washed in Dulbecco's phosphate-buffered saline solution (D-PBS). Cells were recovered by centrifugation and washed with D-PBS. The red blood cells were lysed in 4% acetic acid and the cells were counted using a haemocytometer. Primary hMSC were then seeded at a density of approximately  $2.4\text{--}3.4 \times 10^5$  cells/cm<sup>2</sup> and were maintained in culture for 14 days. Flow cytometry confirmed negative expression of CD45 and positive expression of CD73 and CD105, while hMSC differentiation was confirmed using osteogenic, chondrogenic and adipogenic assays using methods previously described.<sup>[38]</sup>

### **2.3.2 hMSC Metabolism**

Cytotoxicity test methods were employed to examine the cell response in the presence of the CNT/PLA scaffolds as described previously.<sup>[39]</sup> The hMSC were seeded at a density of 20,000 cells/cm<sup>2</sup> and maintained for 24h. at 37C in a humidified atmosphere of 5% CO<sub>2</sub> at 37C. Thereafter, scaffold strips, 1/10 of the total area of the well were placed directly on the cells and incubated for an additional 24 h. An AlamarBlue<sup>TM</sup> (AB) assay (Molecular Probes) was then employed to examine the metabolic activity of the cells by measuring the fluorescence intensity (530nm excitation/590 nm emission) on a microplate fluorescence reader (FLX800, Biotek Instruments Inc.). The percentage viable cells were expressed as a percentage of the AB reduction as per manufacturers instructions. As a method of control, hMSC seeded on tissue culture plastic and hMSC seeded in the presence of PLA nanofibre scaffolds without CNT were also examined (n=6). Cell proliferation was also assessed using a PicoGreen dsDNA quantification fluorescence assay (Molecular Probes, Oregon, USA) (485nm excitation/535 nm emission) on a plate reader (Wallac 1420 Victor 3, Perkin Elmer Inc.)



(n=6).

## 2.4 Statistical Analysis

Where appropriate, results are represented as means  $\pm$  SE. Using the 2-tailed paired student t-test, p-values were determined to compare means between time points and between groups, that is the test CNT/PLA nanofibre scaffolds and the control PLA nanofibre scaffolds, where  $p \leq 0.001$  is shown by \*\*,  $p \leq 0.05$  is represented by \*.

## 3. Results

### 3.1 Effect of CNT on Materials Properties

The chemical structure of the PLA control scaffolds is shown in **Figure 1A** with characteristic peaks at  $2800\text{-}3000\text{cm}^{-1}$  and  $1750\text{cm}^{-1}$  for CH stretching in the  $\text{CH}_3$  group and C=O stretching, respectively.<sup>[24-26]</sup> To examine changes in characteristic peak areas, spectra were normalized to the intensity of the peak at  $1750\text{cm}^{-1}$ . On addition of 2wt% CNT, there was a decrease in peak area for all the characteristic PLA peaks (**Figure 1A**). This change in chemical structure was followed by a change in polymer morphology and mechanical properties, that is, a 5% decrease in polymer crystallinity (**Figure 3C**), a 12% increase in tensile strength (**Figure 4B**), a 5% decrease in percentage elongation (**Figure 4C**) and a 7% increase in modulus (**Figure 4D**) were observed when the CNT were added to the PLA matrix.

### 3.2 Degradation Profile of the CNT/PLA Nanofibre Scaffold

After 7 days in PBS at  $37^\circ\text{C}$ , there was a 3% decrease in the mass of the PLA samples (**Figure 2A**). In parallel, a decrease in the pH of the PBS from 7.3 to 7.2 was observed, indicating increased acidity (**Figure 2B**). There was also a change in the chemical structure of the PLA, as observed in the FTIR spectra (**Figure 1C**). There was a decrease in peak areas

for peaks at  $1080\text{cm}^{-1}$ ,  $1180\text{cm}^{-1}$ ,  $1750\text{cm}^{-1}$ , attributed to C-O-C stretching, C-O, stretching and C=O stretching respectively,  $1360\text{cm}^{-1}$ ,  $1450\text{cm}^{-1}$  attributed to CH bending in the methyl group and  $2950\text{cm}^{-1}$  and  $3000\text{cm}^{-1}$  for CH stretching in the methyl groups. However, it is interesting to note, there were no OH peaks recorded at  $3300\text{cm}^{-1}$ , suggesting that there was no chemically bound water present in the samples. Furthermore, after 7 days, the Tg of the PLA control samples increased from  $63^{\circ}\text{C}$  to  $67^{\circ}\text{C}$  (**Figure 3B**), Tm increased from  $172^{\circ}\text{C}$  to  $174^{\circ}\text{C}$  (**Fig 3C**) and the percentage crystallinity decreased from 49% to 45% (**Fig 3D**), that is, it became more amorphous. This was echoed in the mechanical property data, where the tensile strength increased from 2MPa to 2.7MPa, the percentage elongation decreased from 117% to 75% and Youngs modulus increased from 161MPa to 200MPa.

In contrast, a 17% decrease in mass was observed for the CNT/PLA nanofibre scaffolds (**Figure 2A**) after 7 days in PBS at  $37^{\circ}\text{C}$ . The pH of the PBS solution decreased from 7.3 to 7.2 (**Figure 2B**). In terms of the chemical structure, a decrease in the same peaks as the PLA control was observed in the FTIR spectra (**Fig 1D**). The polymer morphology was also altered with a  $4^{\circ}\text{C}$  increase in Tg from  $63^{\circ}\text{C}$  to  $67^{\circ}\text{C}$  (**Figure 3B**), no change in Tm (**Figure 3C**) and a 9% increase in percentage crystallinity from 44% to 53% (**Figure 3D**). A slight increase from 2.2MPa to 2.3MPa (**Figure 4A**) was recorded for the tensile strength of the CNT/PLA scaffold, while decreases in both the percentage elongation and modulus from 111% to 70% (**Figure 4C**) and 171MPa to 129MPa (**Figure 4D**) were recorded respectively. In terms of p-values for CNT/PLA scaffolds at day 0 and day 7, statistically significant differences were recorded for changes in mass, pH, Tg, percentage crystallinity, percentage elongation and modulus. There were further statistically significant differences observed between the CNT/PLA specimens and the control PLA specimens at day 7 for mass, Tm and crystallinity. However, there were no significant differences between the mechanical properties recorded.

After 14 days, a 4% decrease in the mass of the control PLA samples was observed (**Figure 1A**) and the pH of the solutions became more acidic (**Figure 1B**). However, there was a recovery in the peak areas for the functional groups shown in the FTIR spectra (**Figure 2C**), a decrease in T<sub>g</sub> to 68°C (**Figure 3B**), a decrease in T<sub>m</sub> to 174°C (**Figure 3C**) and an increase in percentage crystallinity to 52% (**Figure 3D**), which may in turn account for the reductions in tensile stress to 2.7MPa (**Figure 4B**), percentage elongation to 75% (**Figure 4C**) and modulus to 201 MPa (**Figure 4D**). In terms of the p-values, statistically significant differences for the PLA control between day 0 and day 14 were recorded for the change in pH, tensile stress, and percentage elongation, where  $p \leq 0.05$ .

Regarding the CNT/PLA nanofibre scaffolds, a further increase in peak areas was observed in the FTIR spectra (**Figure 1D**) after 14 days. The mass of the samples increased by 10% (**Figure 2A**) and the PBS solution again was more acidic, with a further decrease in pH from 7.2 to 6.9 observed (**Figure 2B**). With respect to polymer morphology, T<sub>g</sub> remained relatively unchanged at 67°C (**Figure 3B**), while T<sub>m</sub> and the percentage crystallinity decreased slightly to 172.5°C (**Figure 3C**) and 51% (**Figure 3D**) respectively. In terms of mechanical properties, the tensile strength remained relatively unchanged at 2.4 MPa (**Figure 4B**), the percentage elongation decreased further to 63% (**Figure 4C**) and the modulus remained unaltered at 113MPa (**Figure 4D**). These changes in properties were further highlighted by the p-values recorded, where statistically significant changes between day 0 and day 14 were noted for changes in mass, pH, T<sub>g</sub>, percentage crystallinity, percentage elongation and modulus. However, in terms of differences between the CNT/PLA samples and the control PLA samples, statistically significant differences were only recorded for T<sub>g</sub> at day 14.

After 28 days, the mass of the control PLA sample increased by 1% (**Figure 1A**) and the pH remained unchanged at 7.0 (**Figure 2B**) when compared to values at day 14. A further increase in T<sub>g</sub> was observed from 64.5°C to 67°C (**Figure 3B**), while a very small decrease in T<sub>m</sub> from 173.2°C to 172.8°C (**Figure 3C**) and a 2% increase in the percentage crystallinity (**Figure 3D**) was observed. While the tensile strength and the percentage elongation remain unchanged with values of 2.5MPa (**Figure 4B**) and 64% (**Figure 4C**) recorded respectively, a 38% increase in modulus from 124MPa to 171 MPa (**Figure 4D**) was observed. In comparing the p-values for the PLA samples at day 28 to day 0, there were statistically significant differences recorded in T<sub>g</sub>, percentage crystallinity, tensile strength and percentage elongation.

In comparison, there is a 25% increase in mass of the CNT/PLA specimens after 28 days in PBS (**Figure 2A**) and the pH of the solution increased slightly to 7.0 (**Figure 2B**). The chemical structure also appeared altered with further increases in peak areas. However, T<sub>g</sub> appeared to have plateaued at 68°C (**Figure 3B**), T<sub>m</sub> decreased to 172°C (**Figure 3C**) and the percentage crystallinity remained unchanged at 51% (**Figure 3D**). A slight decrease in tensile strength from 2.4MPa to 2.2 MPa and percentage elongation from 72% to 60% were observed, while as with the controls, the modulus increased by 17% from 113MPa to 132MPa. When comparing the p-values for the CNT/PLA scaffold specimens between day 0 and day 28, statistically significant differences were recorded for mass, pH, T<sub>g</sub>, percentage crystallinity, percentage elongation and modulus. In comparing the test CNT/PLA specimens to the control specimens at day 28, p-values indicated that there were significant differences in mass, T<sub>m</sub> and percentage crystallinity, while there were no statistical differences in mechanical properties. On visible examination of the nanofibre scaffolds using scanning electron microscopy, the difference in the degradation profile observed between the CNT/PLA nanofibre scaffold and the PLA nanofibre control was also evident. When

compared to the control PLA nanofibre scaffolds, the presence of the CNT appeared to enhance the physical stability of the scaffolds, with less degradation visible on the surface of the CNT/PLA nanofibre (**Figure 5**). Furthermore, using Raman spectroscopy, there was no evidence of CNT detected in the PBS solution at any of the time points during the course of the 28-day experiment.

### **3.3 hMSC Viability in the Presence of the CNT/PLA Nanofibre Scaffold**

In order to examine the cytotoxicity of the nanofibre scaffolds, the cell viability was examined using human mesenchymal stem cells (hMSC); an Alamar blue™ assay revealed that there was no statistical difference in the cell metabolism of cells grown on tissue culture plastic (TCP) or cells grown in the presence of the PLA or CNT/PLA nanofibre scaffolds (**Figure 6A**). This is further validated by the dsDNA quantification PicoGreen™ fluorescence assay, which also shows that there is no statistical difference between the numbers of cells grown on TCP or in the presence of either of the nanofibre scaffolds after 24h. (**Figure 6B**).

## **4. Discussion**

As described above, electrical resistance was used a measure to determine the optimum CNT concentration, whereby an inverse relationship between electrical resistance and CNT concentration was observed. Above 2wt% of CNT, the values began to plateau, suggesting the percolation threshold was achieved. This compares well with other studies, where electrical resistance decreases or electrical conductance increases with increase in CNT concentration.<sup>[27]</sup> Furthermore, it was also observed that the chemical, morphological and mechanical properties were altered with the addition of 2wt% CNT to the PLA matrix, that is, a decrease in characteristic PLA peak areas in the FTIR spectra, a 5% decrease in polymer crystallinity, a 17% increase in tensile strength, a 7% increase in modulus and a 5% decrease in the percentage elongation. The change in peak areas observed on addition of the CNT was

similar to that seen in other studies, where CNT nanoparticles were added to PLGA matrices and altered their characteristic peak areas.<sup>[28]</sup> In terms of mechanical properties, it is well known that the addition of CNT to polymer matrices alters polymer chain mobility and mechanical properties, the degree of which is dependent on the CNT concentration.<sup>[29-31]</sup> In terms of traditional polymer composite studies, 2-wt% CNT is at the lower end of the scale, so it is not unexpected that the subsequent improvement in mechanical properties is also at the lower end of the scale. Nonetheless, the trends observed compare well with previous studies.<sup>[29-31]</sup>

As expected after 28 days in PBS at 37°C, the pH of the solution decreases, that is, it becomes more acidic. Although, the general trend in polymer chemistry for both the CNT/PLA nanofibre scaffold and the control PLA nanofibre scaffold are similar, the peak areas at 1360cm<sup>-1</sup> and 1450cm<sup>-1</sup> attributed to the CH bending of the CH<sub>3</sub> group do not recover for the CNT/PLA scaffolds, while all the others are comparable to their values at day 0. Furthermore, the polymer morphology of the two scaffolds stored in the physiological solutions is different. While there is a decrease in the percentage crystallinity and an increase in T<sub>g</sub> for the PLA control, there is an increase in both the percentage crystallinity and T<sub>g</sub> for the CNT/PLA scaffolds after 7 days. However, when the p-values of the CNT/PLA specimens are compared to the p-values for the PLA controls at day 7, there are significant differences in T<sub>m</sub> and the percentage crystallinity. By day 14, the differences between the CNT/PLA specimens and the PLA controls, the differences are less significant, with only differences in T<sub>m</sub> observed. However, by day 28, there are further differences between the morphology of the CNT/PLA scaffolds and the PLA controls, with statistically significant differences observed in T<sub>m</sub> and the percentage crystallinity. Taken together with the chemical structure information, this suggests that there is a change in the conformation of the PLA matrix stored in PBS at 37°C and furthermore the CNT are inhibiting molecular motion and altering the

degradation profile. This is not unexpected as, Armentano et al. saw similar conformational results when SWNT were added to PLGA matrices.<sup>[28]</sup> This is also evident in the SEM images shown in Figure 5, where the surface of the CNT/PLA nanofibre appear more stable when compared to that of PLA control, which also compares favorably with previous *in vitro* degradation studies of PLA nanofibers.<sup>[32,33]</sup> Furthermore, after 28 days in PBS at 37°C, the mechanical properties of the CNT/PLA nanofibre scaffold are similar to that of native tissue.<sup>[35]</sup>

Although, there has been great excitement generated regarding the use of CNT for biomedical applications<sup>[13]</sup>, concern still exists about their cytotoxicity. Indeed, in a separate study, the authors revealed that at low concentrations, SWNT had no adverse affect on hMSC viability, proliferation or indeed differentiation.<sup>[35]</sup> However at higher concentrations, the presence of CNT resulted in cell death. In this study, the authors revealed that there was no statistically significant difference in cell viability or proliferation for hMSC cultured in the presence of the CNT/PLA nanofibre scaffolds, the PLA nanofibre controls or hMSC cultured on tissue culture plastic, which in turn also compares well with other CNT based scaffold studies.<sup>[36]</sup>

## Conclusion

In summary, an electroactive carbon nanotube/polylactic acid based nanofibre scaffold was created by electrospinning. After 28 days in simulated physiological solution at 37°C, the chemical structure and polymer chain conformation were altered, while the solution became more acidic. However, when compared to the control PLA nanofibre scaffolds, the presence of the CNT appears to enhance the physical stability of the scaffolds, with less degradation visible on the surface of the CNT/PLA nanofibers. Furthermore, the CNT containing scaffolds had no adverse cytotoxic effects on the human mesenchymal stem cells. Taken

together, these results auger well for the creation of CNT based scaffolds for tissue engineering electroactive tissue applications.

Acknowledgements: The authors would like to thank Ms. Georgina Shaw for her advice and help with the isolation of the mesenchymal stem cell cells, Ms. Caitriona Liddane and Mr. Gary Kiernan for their help with the electrical conductance measurements. This research has been supported by Science Foundation Ireland Research Frontiers Program (RFP/05/ENG004).

Received: ((will be filled in by the editorial staff)); Revised: ((will be filled in by the editorial staff)); Published online: ((will be filled in by the editorial staff))

- [1] T. Eschenhagen, C. Fink, U. Remmers, H. Scholz, J. Wattchow, J. Weil, W. Zimmermann, H. H. Dohmen, H. Schafer, N. Bishopric, T. Wakatsuki, E. L. Elson, *Faseb J* **1997**, 11, 683.
- [2] I. Kehat, L. Khimovich, O. Caspi, A. Gepstein, R. Shofti, G. Arbel, I. Huber, J. Satin, J. Itskovitz-Eldor, L. Gepstein, *Nature Biotechnology* **2004**, 22, 1282.
- [3] D. Orlic, J. Kajstura, S. Chimenti, D. M. Bodine, A. Leri, P. Anversa, *Annals of the New York Academy of Sciences* **2001**, 938, 221;
- [4] D. Orlic, J. Kajstura, S. Chimenti, F. Limana, I. Jakoniuk, F. Quaini, B. Nadal-Ginard, D. M. Bodine, A. Leri, P. Anversa, *Proceedings of the National Academy of Sciences of the United States of America* **2001**, 98, 10344.
- [5] D. Orlic, J. Kajstura, S. Chimenti, I. Jakoniuk, S. M. Anderson, B. Li, J. Pickel, R. McKay, B. Nadal-Ginard, D. M. Bodine, A. Leri, P. Anversa, *Nature* **2001**, 410, 701.

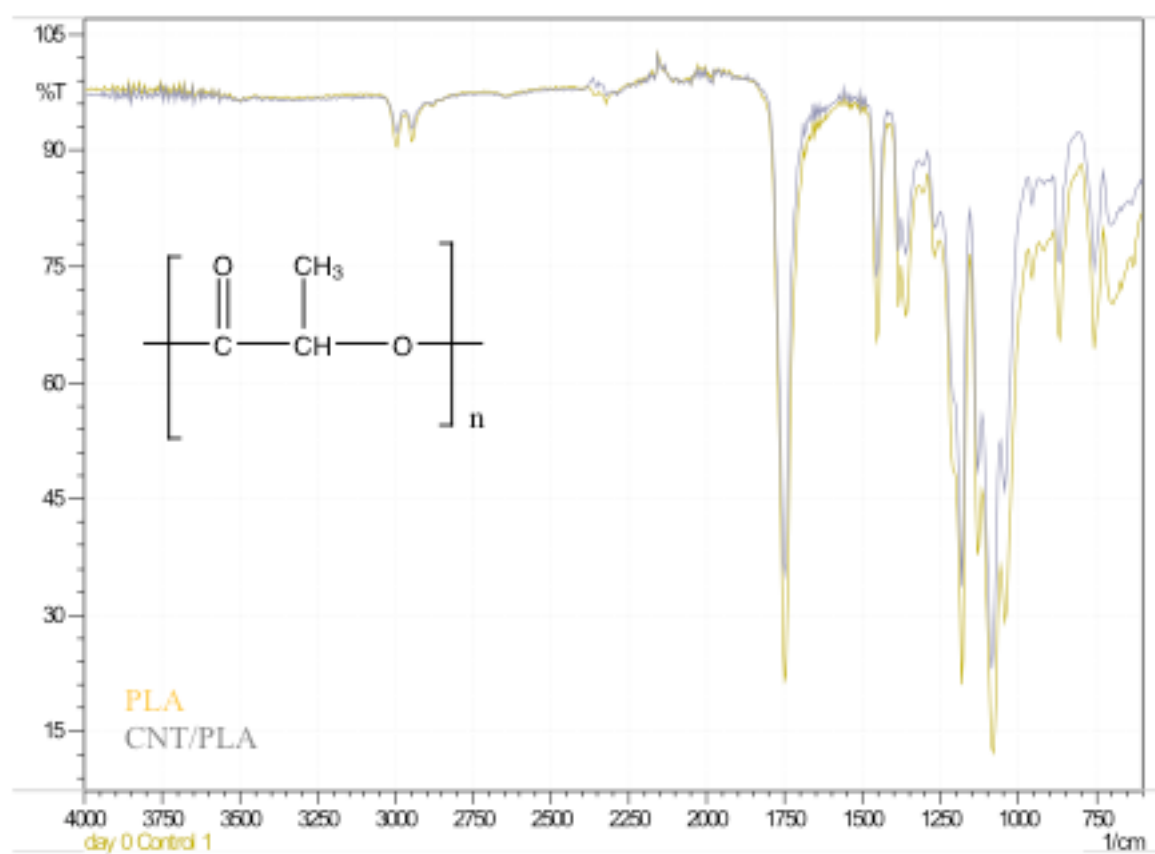


- [6] M. Radisic, H. Park, H. Shing, T. Consi, F. J. Schoen, R. Langer, L. E. Freed, G. Vunjak-Novakovic, Proceedings of the National Academy of Sciences of the United States of America **2004**, 101, 18129.
- [7] J. Satin, I. Kehat, O. Caspi, I. Huber, G. Arbel, I. Itzhaki, J. Magyar, E. A. Schroder, I. Perlman, L. Gepstein, The Journal of Physiology **2004**, 559, 479.
- [8] A. Kawamoto, H. C. Gwon, H. Iwaguro, J. I. Yamaguchi, S. Uchida, H. Masuda, M. Silver, H. Ma, M. Kearney, J. M. Isner, T. Asahara, Circulation **2001**, 103, 634.
- [9] V. Schachinger, B. Assmus, M. B. Britten, J. Honold, R. Lehmann, C. Teupe, N. D. Abolmaali, T. J. Vogl, W. K. Hofmann, H. Martin, S. Dimmeler, A. M. Zeiher, Journal of the American College of Cardiology **2004**, 44, 1690.
- [10] M. T. Valarmathi, R. L. Goodwin, J. W. Fuseler, J. M. Davis, M. J. Yost, J. D. Potts, Biomaterials, **2010** 31, 3185.
- [11] D. Simpson, H. Liu, T. H. Fan, R. Nerem, S. C. Dudley, Jr., Stem Cells **2007**, 25, 2350.
- [12] N. Bursac, M. Papadaki, R. J. Cohen, F. J. Schoen, S. R. Eisenberg, R. Carrier, G. Vunjak-Novakovic, L. E. Freed, The American Journal of Physiology **1999**, 277, H433
- [13] R. L. Carrier, M. Papadaki, M. Rupnick, F. J. Schoen, N. Bursac, R. Langer, L. E. Freed, G. Vunjak-Novakovic, Biotechnology and Bioengineering **1999**, 64, 580;
- [14] L. E. Freed, G. Vunjak-Novakovic, In vitro Cellular & Developmental Biology **1997**, 33, 381.
- [15] N. R. Blan, R. K. Birla, Journal of Biomedical Materials Research **2008**, 86, 195
- [16] L. A. Hidalgo-Bastida, J. J. Barry, N. M. Everitt, F. R. Rose, L. D. Buttery, I. P. Hall, W. C. Claycomb, K. M. Shakesheff, Acta Biomaterialia **2007**, 3, 457;
- [17] H. Park, M. Radisic, J. O. Lim, B. H. Chang, G. Vunjak-Novakovic, In Vitro Cellular & Developmental Biology **2005**, 41, 188

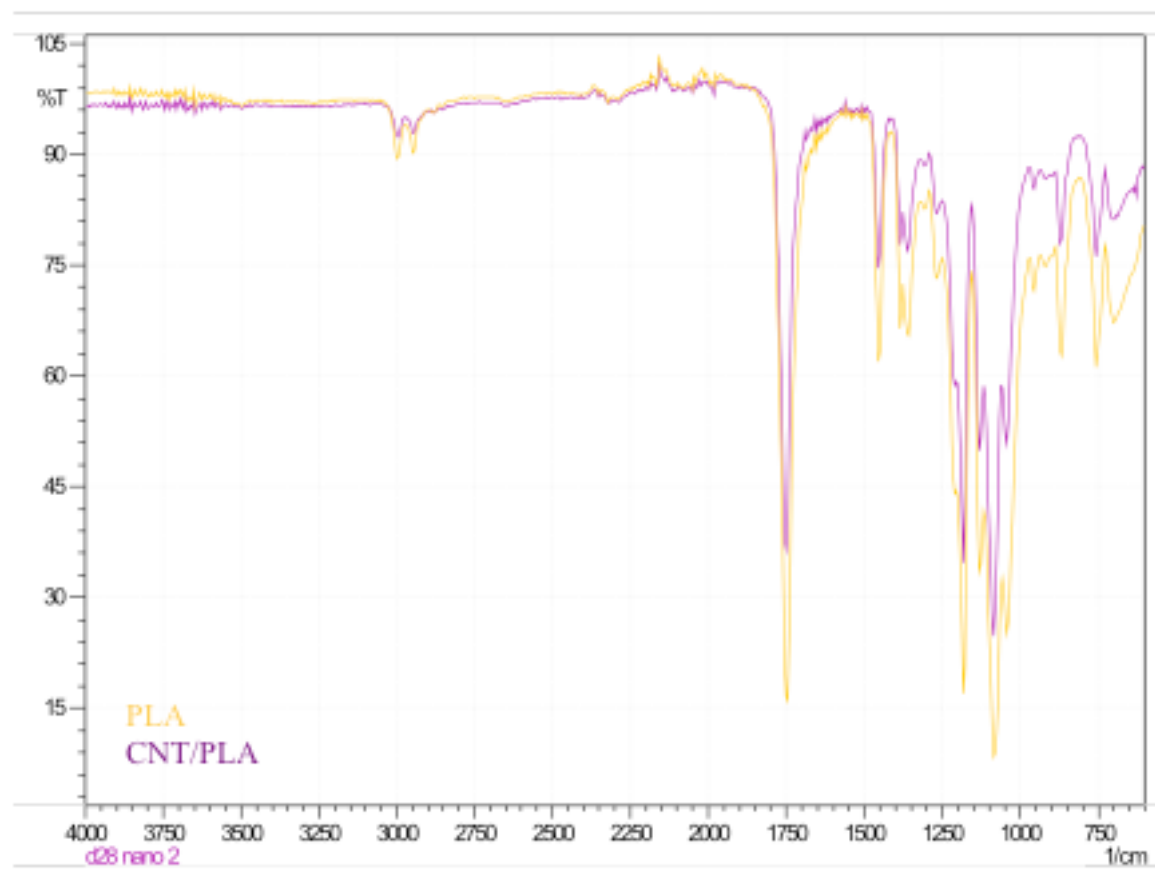
- [18] P. R. Bidez, 3rd, S. Li, A. G. MacDiarmid, E. C. Venancio, Y. Wei, P. I. Lelkes, *Journal of Biomaterials Science* **2006**, 17, 199;
- [19] Y. Guo, M. Li, A. Mylonakis, J. Han, A. G. MacDiarmid, X. Chen, P. I. Lelkes, Y. Wei, *Biomacromolecules* **2007**, 8, 3025;
- [20] L. Huang, J. Hu, L. Lang, X. Wang, P. Zhang, X. Jing, X. Wang, X. Chen, P. I. Lelkes, A. G. MacDiarmid, Y. Wei, *Biomaterials* **2007**, 28, 1741;
- [21] M. Li, Y. Guo, Y. Wei, A. G. MacDiarmid, P. I. Lelkes, *Biomaterials* **2006**, 27, 2705;
- [22] Y. Wan, A. Yu, H. Wu, Z. Wang, D. Wen, *Journal of Materials Science* **2005**, 16, 1017.
- [23] B. S. Harrison, A. Atala, *Biomaterials* **2007**, 28, 344.
- [24] D. Blond, W. Walshe, K. Young, F. Blighe, U. Khan, D. Almecija, L. Carpenter, J. McCauley, W. Blau, J. Coleman, *Adv. Funct. Mater.* **2008**, 18, 2618.
- [25] W. Jang, Y. Boo, J. Tae, R. Narayan, *J. Ind. Eng. Chem* **2007**, 13, 457;
- [26] E. Pamula, M. Blazewicz, C. Paluszkiwicz, P. Dobrzynski, *Journal of Molecular Structure* **2001**, 596, 69;
- [27] P. Thanki, E. Dellacherie, J.-L. Six, *Applied Surface Science* **2006**, 253, 2758.
- [28] H. S. Kim, H. I. Kwon, S. M. Kwon, Y. S. Yun, J. S. Yoon, H. J. Jin, *Journal of Nanoscience and Nanotechnology*, **2010**, 10, 3576.
- [29] B. Armentano, M. Dottori, D. Puglia, J. M. Kenny, *Journal of Materials Science* **2008**, 19, 2377.
- [30] M. Cadek, J. N. Coleman, V. Barron, K. Hedicke, W. J. Blau, *Applied Physics Letters* **2002**, 81, 5123.
- [31] K. Sahithi, M. Swetha, K. Ramasamy, N. Srinivasan, N. Selvamurugan, *International Journal of Biological Macromolecules*, **2010**, 46, 281.
- [32] Y. Dong, S. Liao, M. Ngiam, C. K. Chan, S. Ramakrishna, *Tissue Engineering* 2009, 15, 333

- [33] D. Ishii, T. H. Ying, A. Mahara, S. Murakami, T. Yamaoka, W. K. Lee, T. Iwata, *Biomacromolecules* **2009**, 10, 237.
- [34] H. Saraf, K. T. Ramesh, A. M. Lennon, A. C. Merkle, J. C. Roberts, *Journal of Biomechanics* **2007**, 40, 1960.
- [35] E. Mooney, P. Dockery, U. Greiser, M. Murphy, V. Barron *Nano Lett.*, **2008**, 8, 8, 2137
- [36] D. Lahiri, F. Rouzaud, S. Namin, A. K. Keshri, J. J. Valdes, L. Kos, N. Tsoukias, A. Agarwal, *Applied Materials & Interfaces* **2009**, 1, 2470.
- [37] M. Day, A Victoria Nawaby, X Liao, *Journal of Thermal Analysis and Calorimetry* **2006**, 86, 3, 623.
- [38] J. M. Murphy, K. Dixon, S. Beck, D. Fabian, A. Feldman, F. Barry, *Arthritis and Rheumatism* **2002**, 46, 704.
- [39] M. A. Punchard, Stenson-Cox C., O'cearbhaill E.D., Lyons E., Gundy S., Murphy L., Pandit A., McHugh P.E., Barron V.. *J Biomech.* **2007**, 40, 14, 3, 146

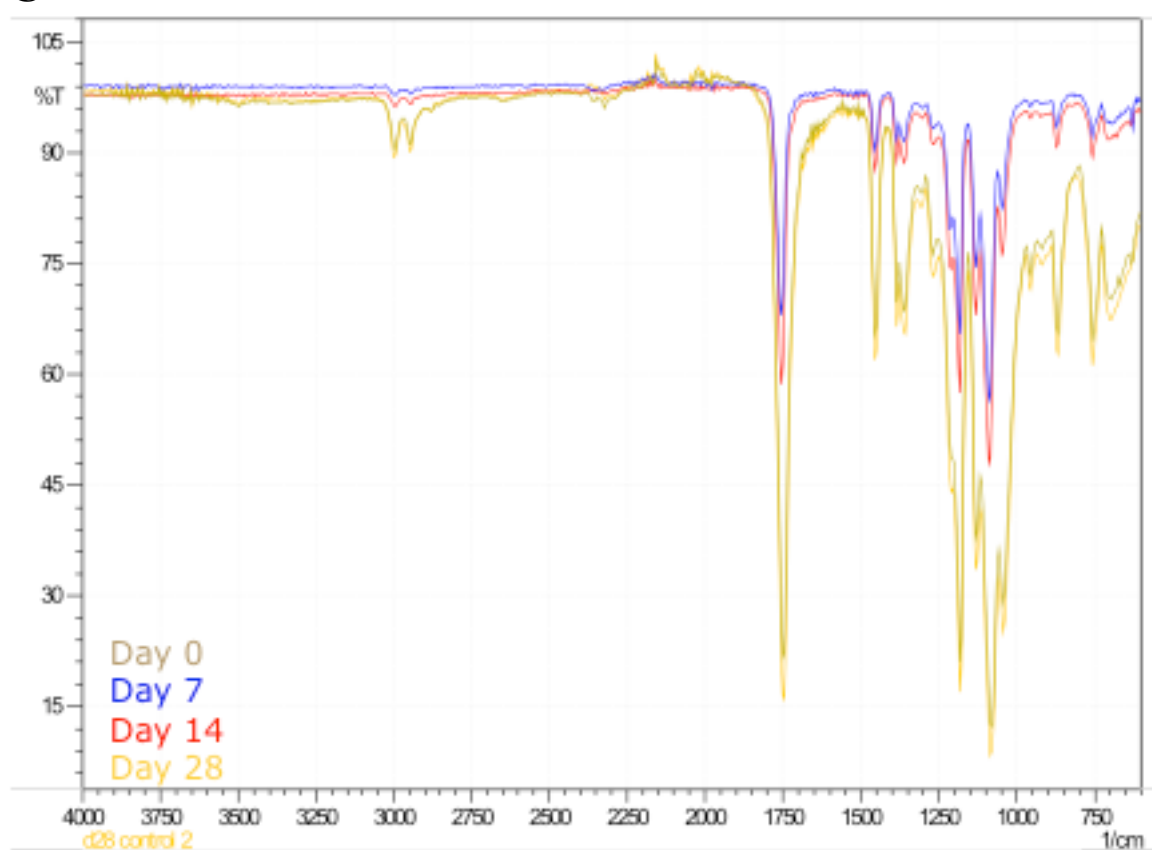
A



**B**

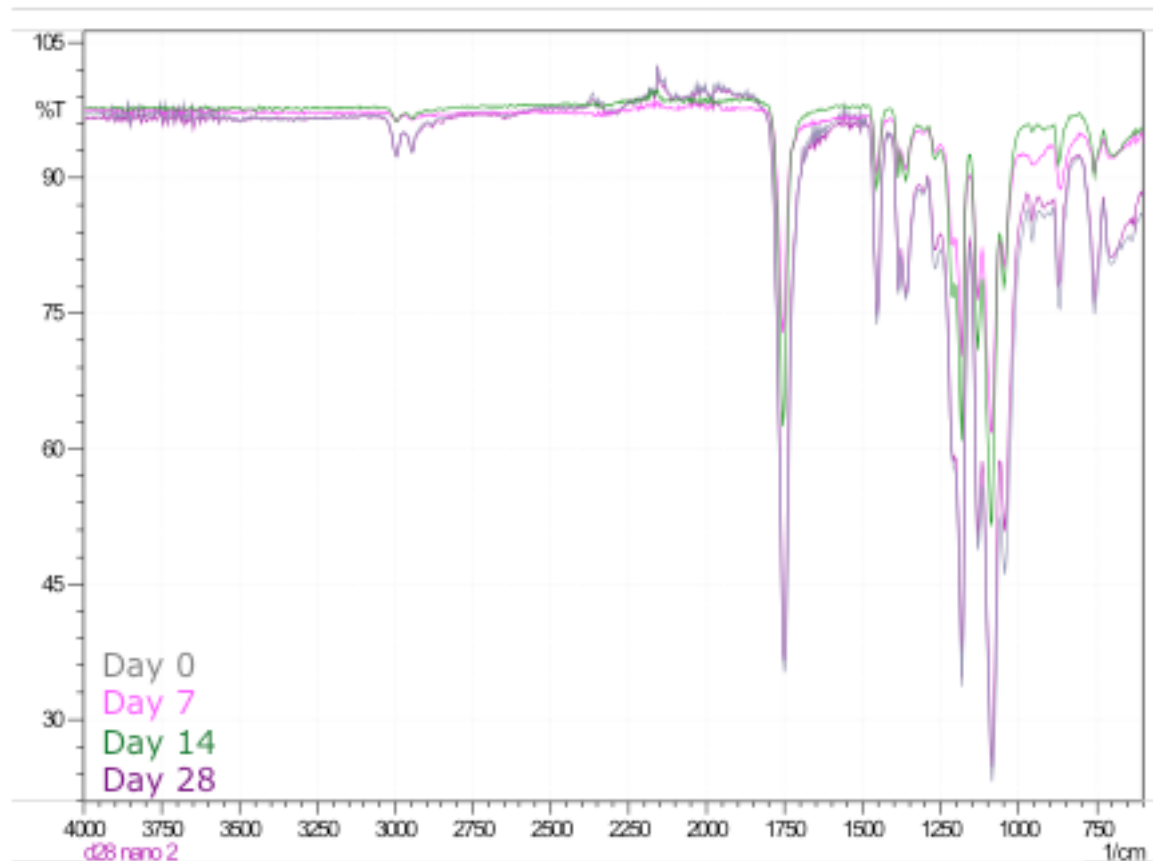


C



Time (days)	Peak Areas at Specific Wavelength Numbers (cm <sup>-1</sup> ) for Control PLA						
	1080	1180	1360	1450	1750	2950	3000
0	35.09	18.32	6.189	5.543	24.885	1.666	1.857
7	8.35	4.436	1.361	1.234	5.616	2.043	0.309
14	10.882	5.863	11.334	12.44	7.771	0.561	0.674
28	39.754	19.812	6.888	5.999	29.119	1.945	1.943

**D**

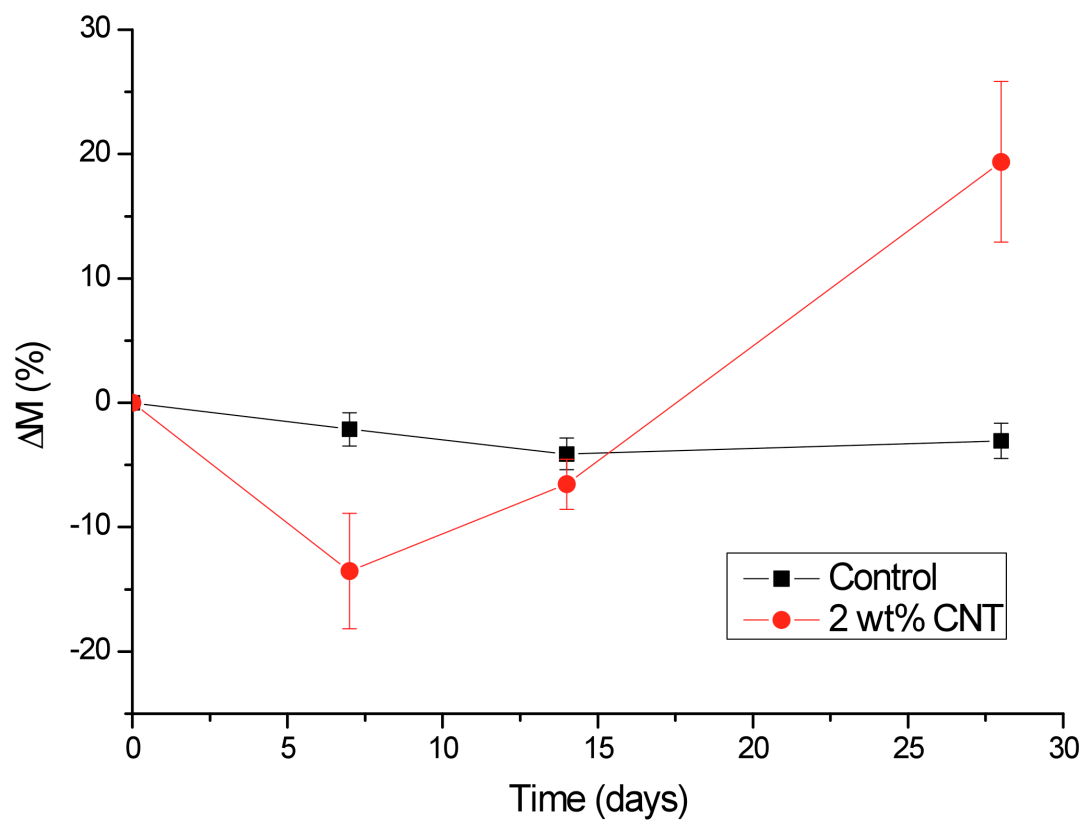


Time (days)	Peak Areas at Specific Wavelength Numbers for CNT/PLA ( $\text{cm}^{-1}$ )						
	1080	1180	1360	1450	1750	2950	3000
0	23.82	12.811	23.405	26.247	16.363	1.69	1.491
7	7.807	4.189	1.532	1.449	4.905	0.265	0.572
14	9.846	5.259	1.704	1.534	6.849	0.146	0.713
28	22.367	11.693	4.198	3.643	16.285	1.628	1.329

**Figure 1.** FTIR spectra showing chemical structure of (A) PLA control and CNT/PLA nanofibre scaffolds with peaks at  $1080\text{cm}^{-1}$ ,  $1180\text{cm}^{-1}$ ,  $1750\text{cm}^{-1}$ , attributed to C-O-C stretching, C-O, stretching and C=O stretching respectively,  $1360\text{cm}^{-1}$ ,  $1450\text{cm}^{-1}$  attributed to CH bending in the methyl group and  $2950\text{cm}^{-1}$  and  $3000\text{cm}^{-1}$  for CH stretching in the methyl groups. (B) Comparison of PLA control and CNT/PLA nanofibre scaffold samples stored in physiological solution at  $37^{\circ}\text{C}$  after 28 days. (C) FTIR spectra and calculated peak area values at specific wavelength numbers for PLA control and (D) CNT/PLA nanofibre scaffold samples stored in physiological solution at  $37^{\circ}\text{C}$  over a 28-day period. Spectra were recorded in ten different areas of each specimen ( $n=6$ ) and normalized to the intensity of peak at  $1450\text{cm}^{-1}$  for CH stretching in the  $\text{CH}_3$  group.

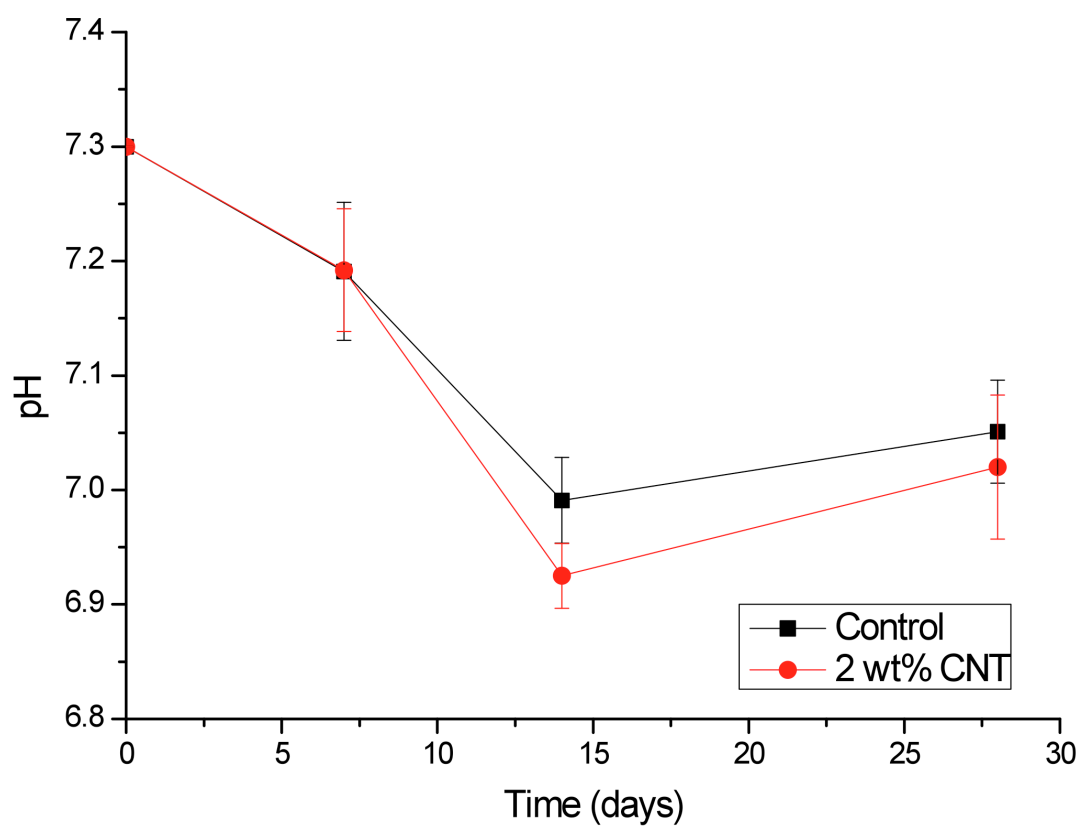


**A**



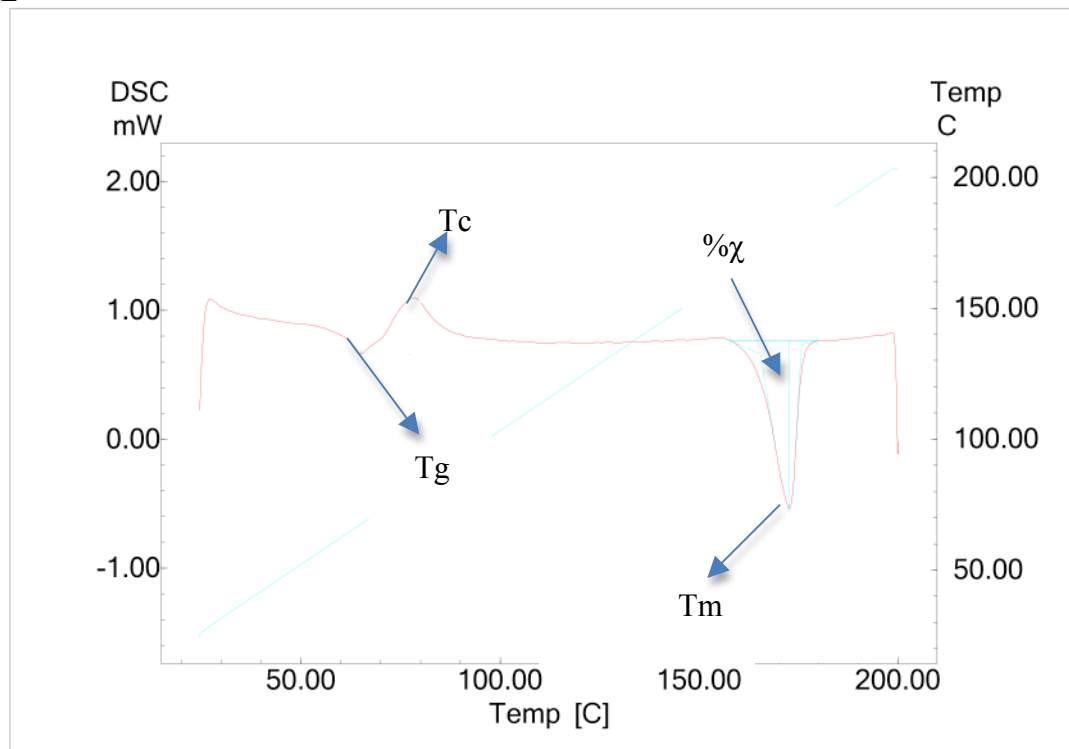
Time (days)	0-7	0-14	0-28
Control	-	-	-
CNT	**	**	*

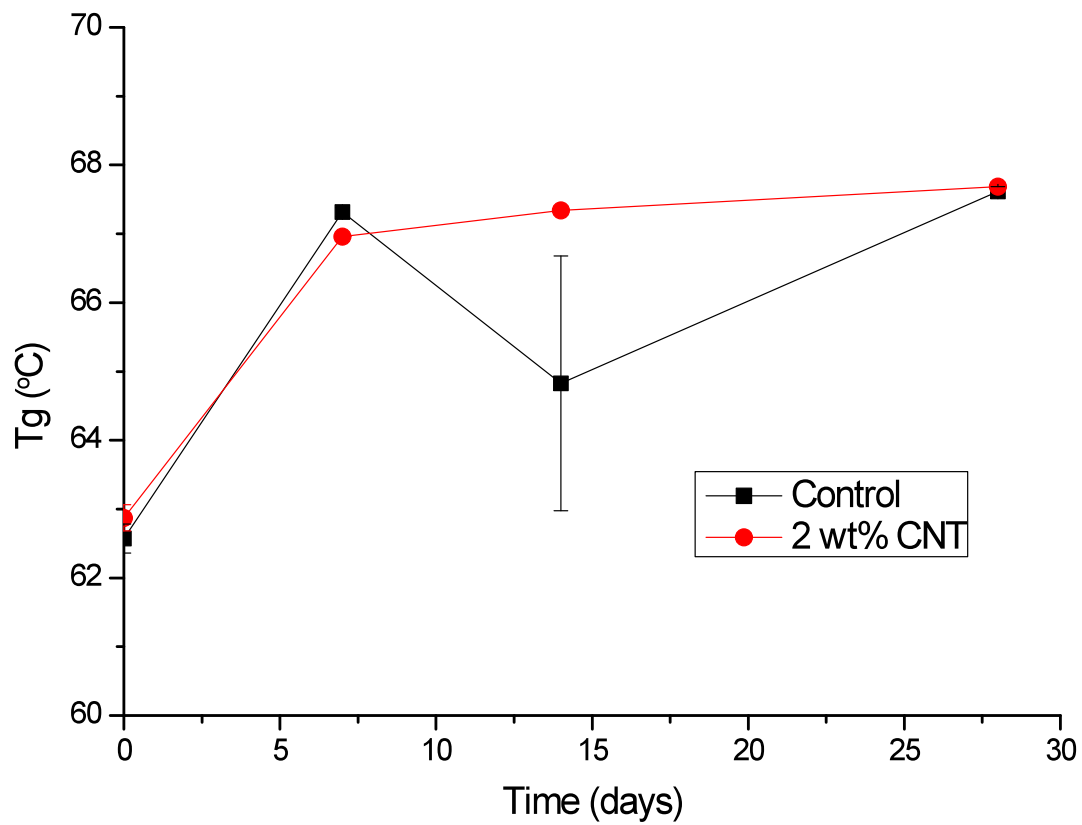
Time (days)	7-7	14-14	28-28
Control vs CNT	**	-	*

**B**

Time (days)	0-7	0-14	0-28
Control	*	*	-
CNT	*	**	**
Time (days)	7-7	14-14	28-28
Control vs CNT	-	-	-

**Figure 2** (A) Change in mass of CNT/PLA scaffold and PLA control samples stored in simulated physiological solutions at 37°C over a 28-day period. (B) pH of solutions containing CNT/PLA scaffold and PLA control samples. Using the 2-tailed paired student t-test, p-values were determined to compare means between time points and between groups, where  $p \leq 0.001$  is shown by \*\*,  $p \leq 0.05$  is represented by \* and – shows that there is no statistical difference (n=10).

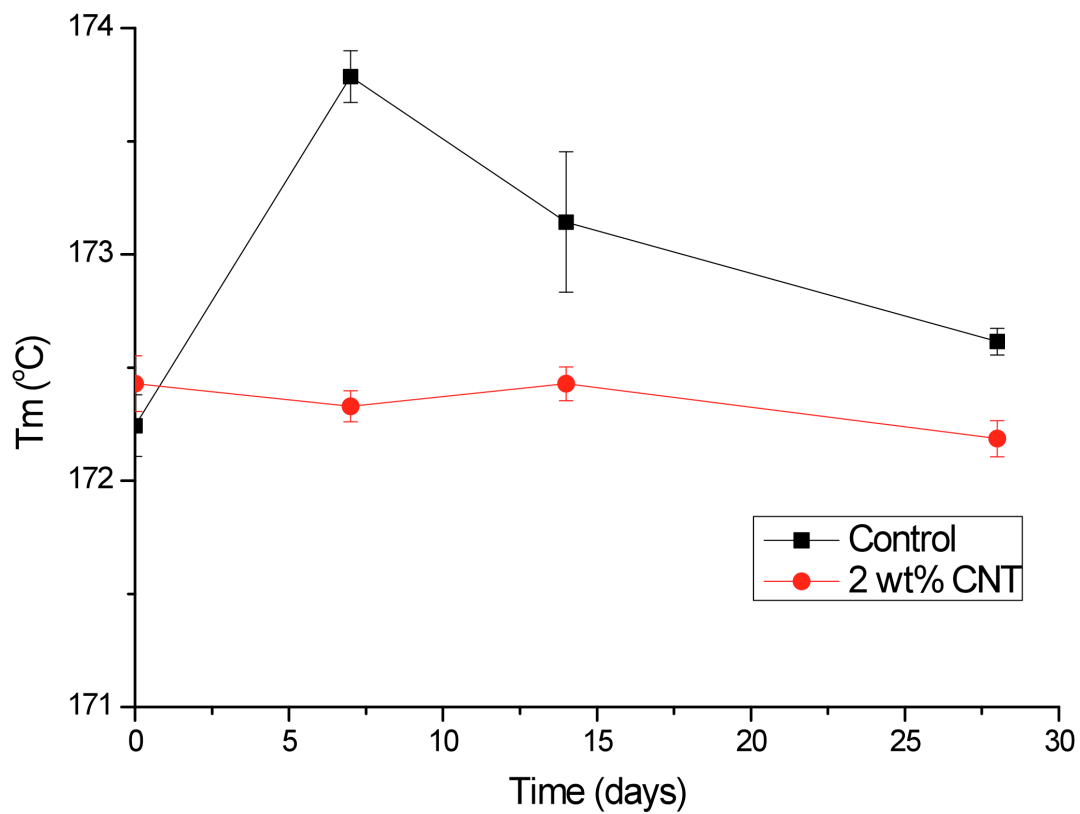
**A**

**B**

Time (days)	0-7	0-14	0-28
Control	**	-	**
CNT	**	**	**

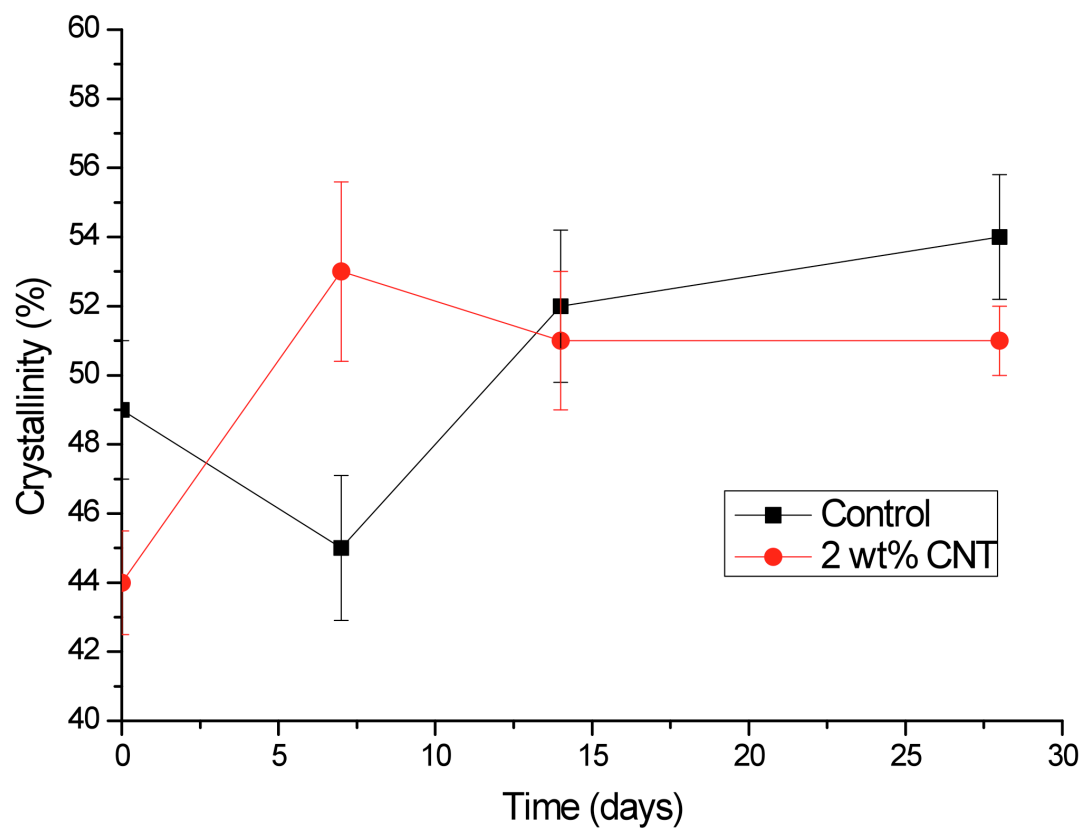
Time (days)	7-7	14-14	28-28
Control vs CNT	-	*	-

**C**



Time (days)	0-7	0-14	0-28
Control	**	-	-
CNT	-	-	-
Time (days)	7-7	14-14	28-28
Control vs CNT	**	-	*

**D**

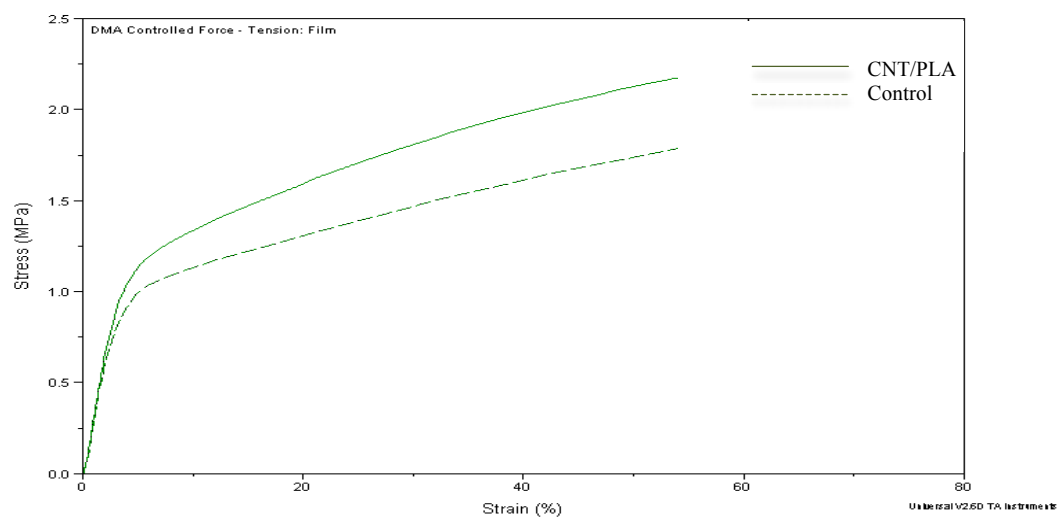


Time (days)	0-7	0-14	0-28
Control	-	-	*
CNT	**	**	**
Time (days)	7-7	14-14	28-28
Control vs CNT	**	-	*

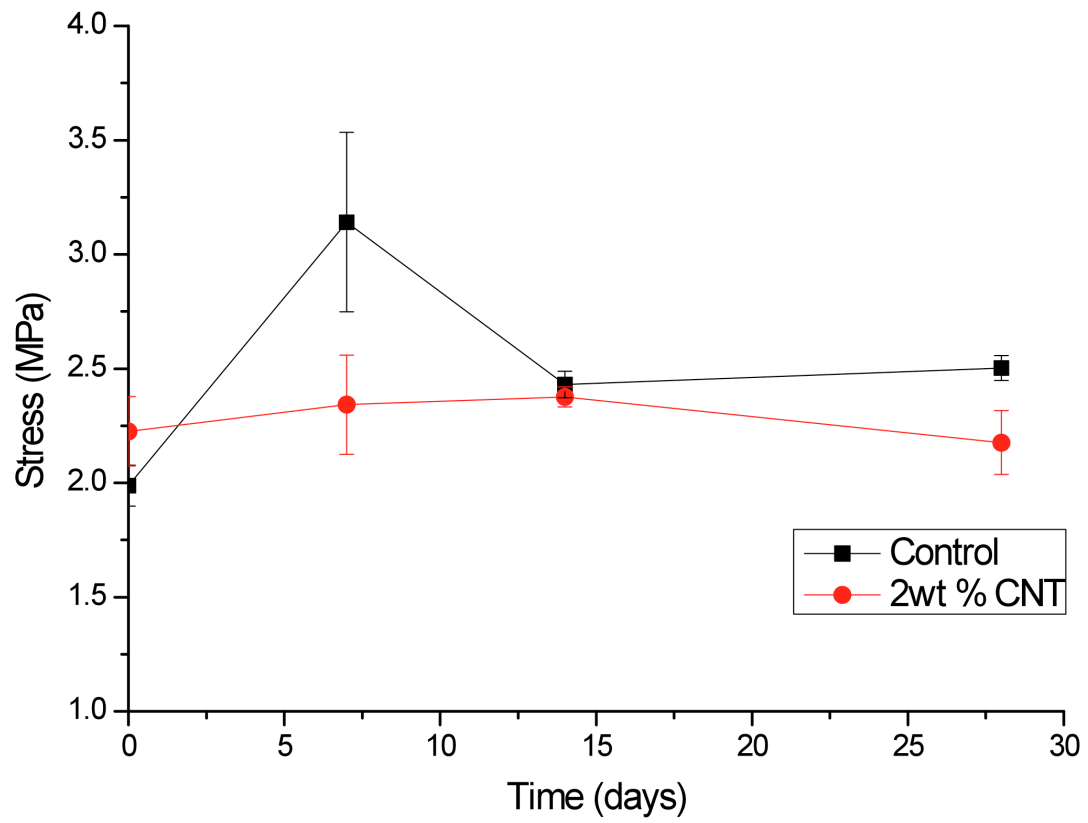
**Figure 3.** (A) Typical DSC thermogram for CNT/PLA scaffold specimens. (B) Change in glass transition temperature of specimens stored in physiological solution at 37°C over 28 days. (C) Change in crystalline melt temperature of specimens stored in physiological solution at 37°C over 28 days. (D) Change in percentage crystallinity of specimens stored in physiological solution over a 28-day period. Using the 2-tailed paired student t-test, p-values were determined to compare means between time points and between groups, where  $p \leq 0.001$  is shown by \*\*,  $p \leq 0.05$  is represented by \* and – shows that there is no statistical difference (n=6).



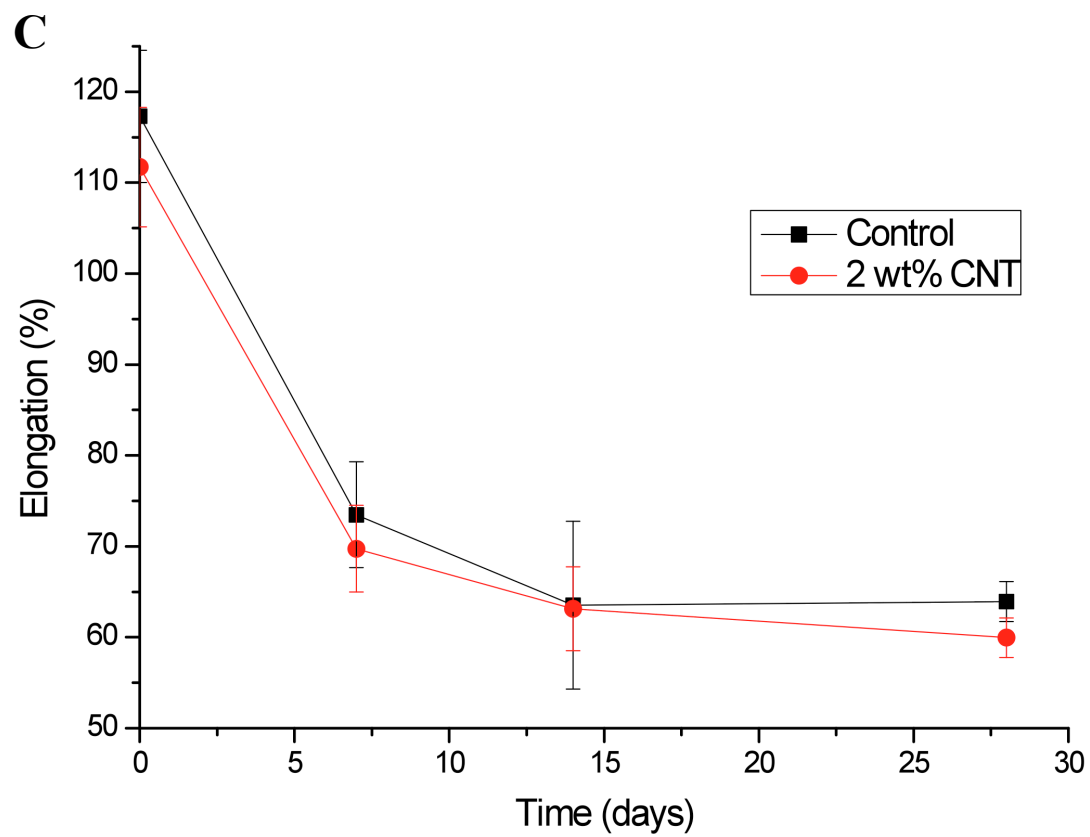
**A**



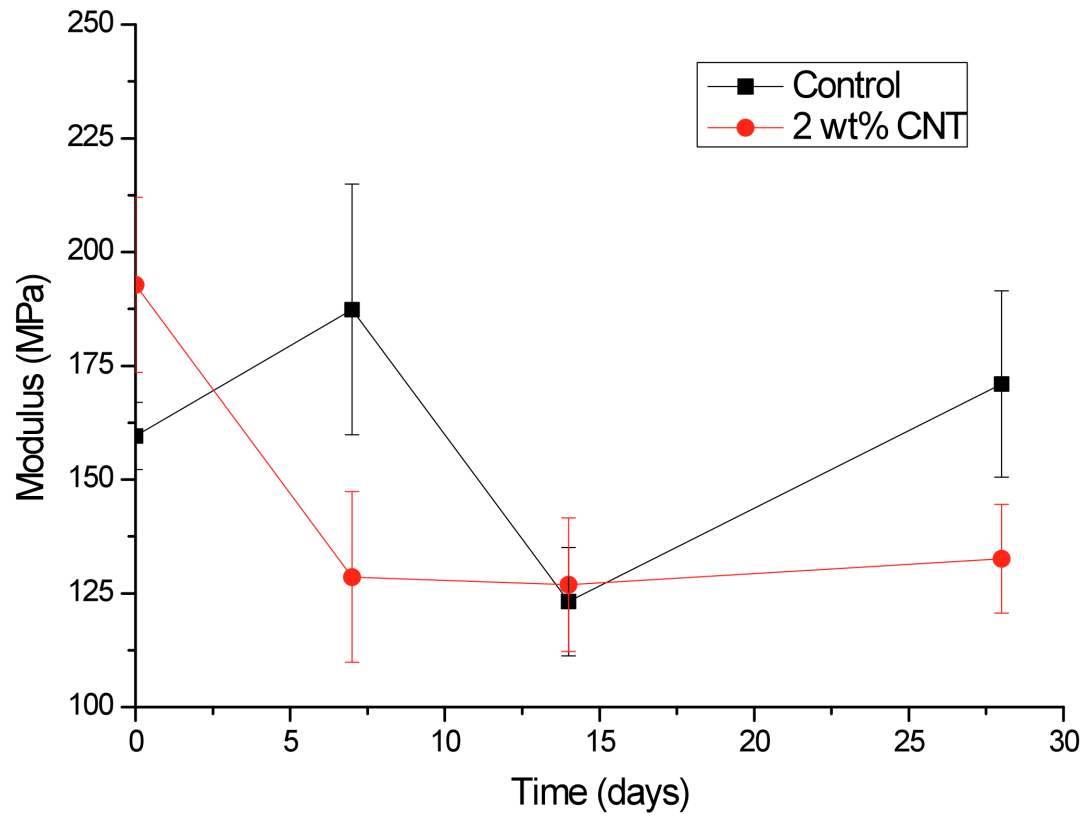
**B**



Time (days)	0-7	0-14	0-28
Control	*	*	*
CNT	-	-	-
Time (days)	7-7	14-14	28-28
Control vs CNT	-	-	-



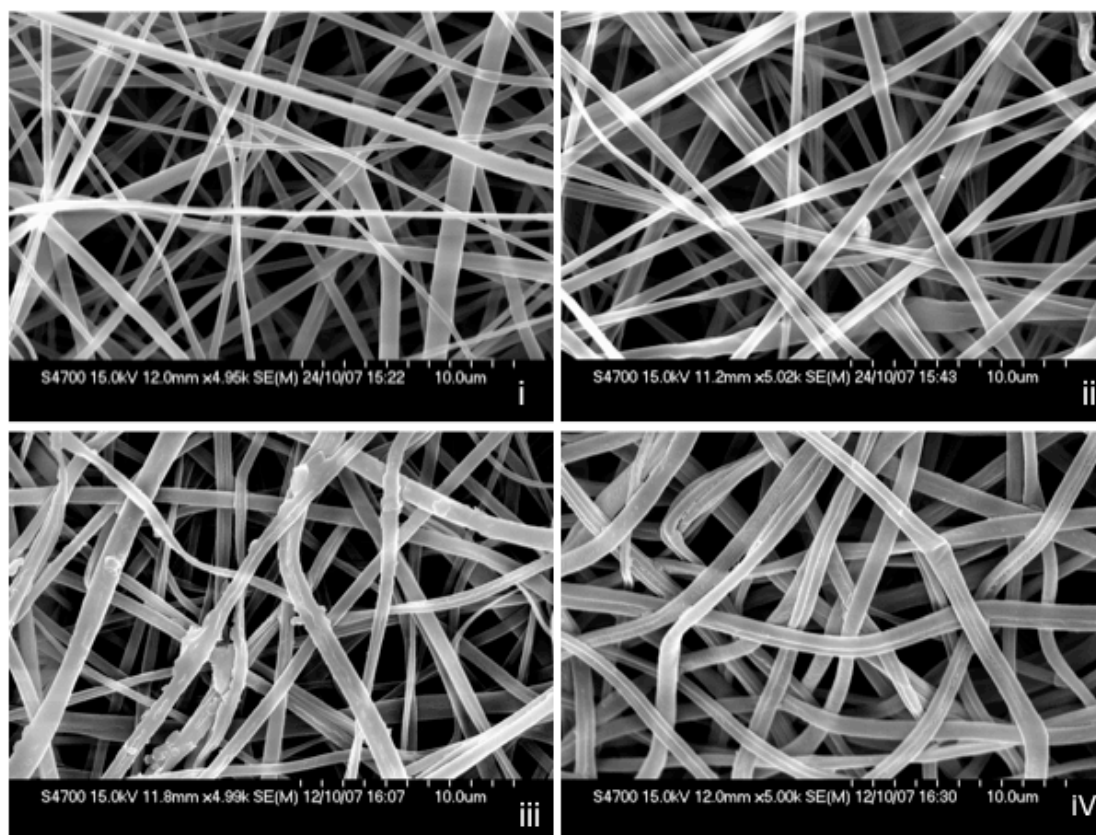
Time (days)	0-7	0-14	0-28
Control	**	*	**
CNT	**	**	**
Time (days)	7-7	14-14	28-28
Control vs CNT	-	-	-

**D**

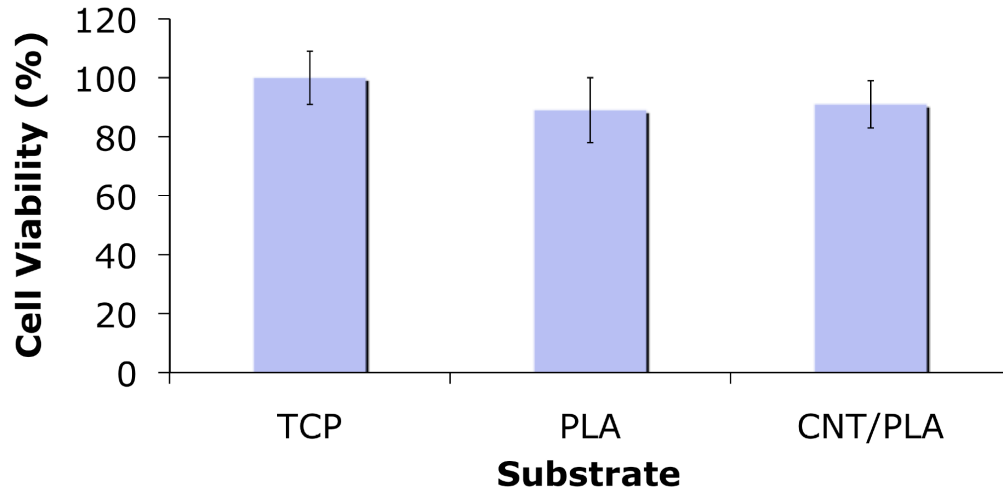
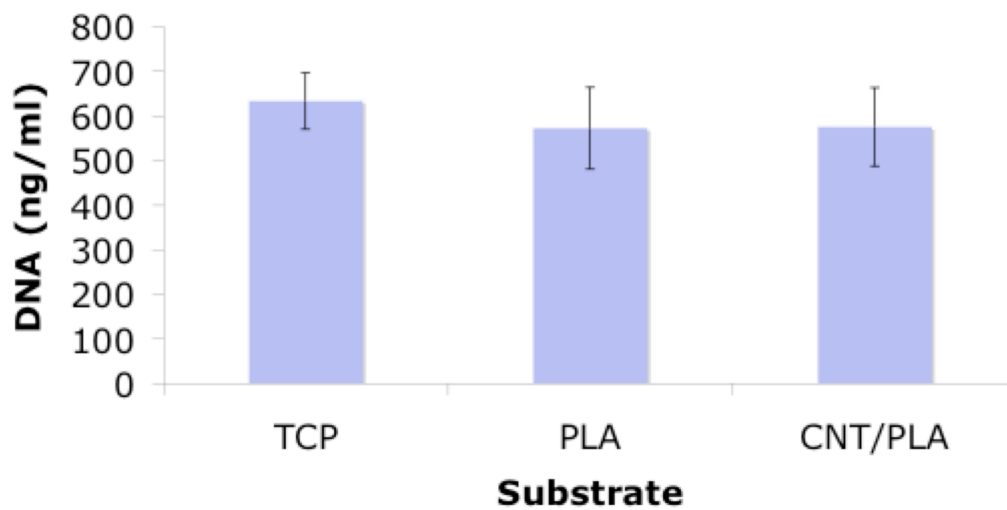
Time (days)	0-7	0-14	0-28
Control	-	-	-
CNT	*	*	*

Time (days)	7-7	14-14	28-28
Control vs CNT	-	-	-

**Figure 4.** (A) Typical stress-strain graph for CNT/PLA and PLA specimens. (B) Change in tensile strength of specimens stored in physiological solution at 37°C over a 28-day period. (C) Change in the percentage elongation of specimens stored in physiological solution at 37°C over a 28-day period. (D) Change in modulus of specimens stored in physiological solution at 37°C over a 28-day period. Using the 2-tailed paired student t-test, p-values were determined to compare means between time points and between groups, where  $p \leq 0.001$  is shown by \*\*,  $p \leq 0.05$  is represented by \* and – shows that there is no statistical difference (n=6).



**Figure 5.** SEM examination of (i) PLA nanofibre scaffold on Day 0, (ii) CNT/PLA nanoscaffold on Day 0, (iii) PLA nanofibre scaffold on 28, (ii) CNT/PLA nanoscaffold on Day 28.

**A****Cell Metabolism****B****Cell Proliferation**

**Figure 6.** (A) Cell metabolism of hMSC grown on tissue culture plastic, PLA and CNT/PLA nanofibre scaffolds after 24h. Cell viability is determined using an Alamar blue assay™. (B) Cell proliferation of hMSC grown on tissue culture plastic, PLA and CNT/PLA nanofibre scaffolds. Cell number is determined using a PicoGreen dsDNA fluorescence assay. Using the 2-tailed paired student t-test, p-values were determined to compare means values between

groups. There is no significant statistical difference between the PLA, the CNT/PLA samples and the cells grown on TCP  $P \geq 0.05$ .



## **The table of contents entry**

**In this study, an electroactive carbon nanotube (CNT) polylactic acid scaffold is created and characterized.** The degradation profile after immersion in simulated physiological solutions at 37°C over a 28-day period is described, where the CNT appear to stabilize the mechanical properties and physical integrity of the scaffold. Furthermore, human mesenchymal stem cells grown in the presence of this electroactive scaffold show no adverse cytotoxic response.

Joseph N. Mackle<sup>1</sup>, David J-P Blond<sup>2</sup>, Caitlin McDonnell<sup>1</sup>, Werner J. Blau<sup>2</sup>, Emma Mooney<sup>1</sup>, Frank Barry<sup>1</sup> Mary Murphy<sup>1</sup> and Valerie Barron\*<sup>1</sup>

**Title *In vitro* Characterization of an Electroactive Carbon Nanotube Based Nanofiber Scaffold For Cardiac Muscle Repair**

ToC figure

